Comparative metrics of advanced serial/parallel biped design and characterization of the main contemporary architectures

Virgile Batto, Thomas Flayols, Nicolas Mansard, Margot Vulliez

Comparative metrics of advanced serial/parallel biped design and characterization of the main contemporary architectures

Virgile Batto[1,2,*] , Thomas Flayols[1,3], Nicolas Mansard[1,3], Margot Vulliez[2]

***Abstract*— The best achievements in bipedal locomotion have resulted from associating an intelligent and efficient design with clever and robust control. While several control frameworks exist, the design of the legs of our biped robots still lacks a systematic approach and remains a crucial challenge for robot mobility. This paper introduces several criteria to characterize the design of bipedal legs. They aim to guide the design choices and could be implemented in a codesign approach. They reflect the leg overall performances (ability to produce dynamic and accurate foot movements, absorb impacts, lower the motor torques needed to stand up) and characterize the design compactness. We give the algorithmic formulations to evaluate them beyond classical serial designs, to account for any parallel mechanisms. To validate these criteria, we developed a library of open-source CAD models describing the main existing biped architectures, which can be used as a database for future design studies. We discuss the comparative performances of these architectures. We hope this quantified discussion can serve as a baseline to better design future biped robots.**

I. Introduction

Many recent advances in locomotion have partly resulted from improvements in hardware. Early robots like M2V2[1], Mabel [2], EP-War3 [3] have been able to respectively walk, run and climb stairs relatively easily. These robots have opened the way to new improved robots able to be more dynamic, like Digit [4], Kangaroo [5], and Atlas [6]. The progress in the design was predominantly based on intuition, i.e., trials and errors. Digit is the successor of Cassie [7] and Atrias [8], and is still being improved in his latest version, where the elastic component has been removed. In particular, parallel mechanisms are promising for developing dynamic robots, as the actuators can be placed closer to the hip of the robot. The designers of Cassie proved such dynamic performances since its serial-parallel architecture makes it run 100m in less than 30s.

Optimization of the architecture is a crucial step when designing a robot. Although yet mostly performed for manipulator robots, either the robot topology [9] or the complete architecture are optimized by codesign, i.e., simultaneously simulating and optimizing the robot hardware and control [10], [11]. For manipulators, classical performance criteria [12], [13] typically involve the dexterity and the workspace [14], or the energy efficiency [15]. Some specific criteria have been proposed to characterize legged robot performance accurately. The impact mitigation factor was proposed for quadrupeds [16] and we will extend it to bipeds in the following sections. The centroidal momentum matrix [17] was proposed to evaluate the stability of biped robots. However, a lack of specific but comprehensive criteria to design and evaluate humanoid robot legs has been spotted.

This paper sets the root of a systematic method to design a bipedal robot's kinematic architecture and actuator placement. We propose several criteria to evaluate the biped performances, and write generic formulations that can evaluate these metrics for legs with parallel mechanisms. We also produce a library of 5 state-of-the-art legged designs, ranging from classical serial walking robots to more dynamic parallel architectures, reported in Fig. 1. The proposed CAD models are unified in format and scaling and released in open source. We validate the relevance of the proposed metrics by discussing the relative advantages of these architectures.

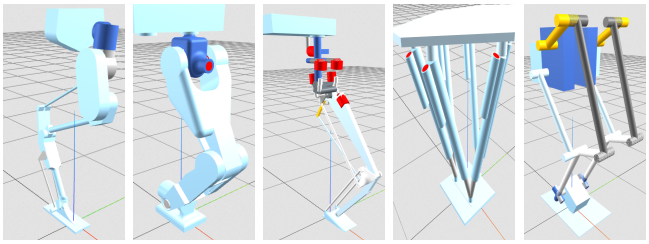

(a) **(b)** **(c)** **(d)** **(e)**

Fig. 1. Examples of advanced leg design: **(a)** Digit [4], **(b)** Talos [19], **(c)** Kangaroo [5], **(d)** WL16 [20], and **(e)** the Disney bipedal robot [21].

II. Background

A. Kinematics

We denote by $q \in \mathbb{R}$ the robot configuration. Assuming the robot is not over-actuated, and the actuators are bounded to avoid non-mountable configurations, the joints can be separated between actuated q_a and free q_f joints $q = (q_a, q_f)$. The same separation is made for the joint forces: $\tau = (\tau_a, \tau_f)$ (disregarding the free-flyer for now).

The parallel mechanism is modeled by the implicit constraint $\phi(q) = 0$. It might be more convenient to express it explicitly, i.e., as f such that $q_f = f(q_a)$. However, in general, only the implicit constraint ϕ can be evaluated, f is not available in closed form, and no automatic conversion exists. As we want each proposed criterion to work for the most common shape, we only consider ϕ to be available and we show how the derivative of f can be obtained or approximated from ϕ, which is the only needed quantity. The fundamental link between implicit and explicit writings

*This work is suported by (1) Défi clé Robotique centrée sur l'humain (funded by Région Occitanie, France), (2) ROBOTEX 2.0 (ROBOTEX ANR-10-EQPX-44-01 and TIRREX-ANR-21-ESRE-0015), (3) Dynamograde (ANR-21-LCV3-0002) and (4) ASAP-HRC (ANR-21-CE10-0002)

[1] LAAS-CNRS, Université de Toulouse, CNRS, Toulouse, France
[2] Auctus, Inria, centre de l'Université de Bordeaux, Talence, France
[3] Artificial and Natural Intelligence Toulouse Institute, France
* corresponding author: virgile.batto@laas.fr

is $\forall q_a, \phi(q_a, f(q_a)) = 0$. Then, thanks to the implicit function theorem:

$$\frac{\partial \phi}{\partial q_a} + \frac{\partial \phi}{\partial f}\frac{\partial f}{\partial q_a} = 0 \tag{1}$$

Assuming $\frac{\partial \phi}{\partial f}$ is full-column rank ie ${\frac{\partial \phi}{\partial f}}^{+}\frac{\partial \phi}{\partial f} = \mathbb{I}$, we get:

$$\frac{\partial q}{\partial q_a} = \begin{bmatrix} \mathbb{I} \\ -{\frac{\partial \phi}{\partial f}}^{+}\frac{\partial \phi}{\partial q_a} \end{bmatrix} \tag{2}$$

The left-inverse [29] of $\frac{\partial \phi}{\partial f}$ is not always unique, notably when internal degrees of freedom exist. The pseudo inverse is nevertheless meaningful in that case, as it minimizes such internal movements and corresponds to a relevant approximation. The operation is exact for most of the existing designs, in particular for the five robots of our library.

B. Operational frame

We consider the *operational* frame $\mathscr{F}_A$ to be attached to the tip of the foot, of particular interest when computing biped performance criteria. The placement of $\mathscr{F}_A$ wrt. the world frame $\mathscr{F}_o$ is denoted by ${}^oM_A(q) \in SE(3)$, which is a function of the configuration q. We have:

$$J_A = T_{q_a}\,{}^oM_A = T_q\,{}^oM_A\frac{\partial q}{\partial q_a} \tag{3}$$

with $T_q\,{}^oM_A$ the tangent application (derivative) of ${}^oM_A(q)$, which corresponds to the classical robot Jacobian of the underlying open chain, for example, computable with a standard tool such as Pinocchio [27], and J_A the equivalent Jacobian acknowledging for the close-loop constraint ϕ.

C. Inertia

The robot dynamics can be written through the constrained Lagrangian form following [28]:

$$M\ddot{q} + b = {\frac{\partial \phi}{\partial q}}^{T}\lambda + \tau \quad \text{s.t} \quad \frac{\partial \phi}{\partial q}\ddot{q} + \frac{\partial \dot{\phi}}{\partial q}\dot{q} = 0 \tag{4}$$

with M the mass matrix, b the nonlinear effects (Coriolis, centrifugal, gravity), and λ the forces exerted by the closed-loop mechanisms. For serial chains, the effective inertia of the foot $\mathscr{F}_A$ is [25]:

$$\Lambda = \left((T_q\,{}^oM_A)\,M^{-1}\,(T_q\,{}^oM_A)^T\right)^{-1} \tag{5}$$

In what follows, we will need an equivalent quantity accounting for the constraint ϕ. We first project (4) on q_a.

$$M_a\ddot{q}_a + b_a = \tau_a \tag{6}$$

assuming the existence of equivalent mass M_a and drift b_a linking $\ddot{q}_a$ to τ_a. To find M_a we write the robot kinetic energy:

$$E_c = \frac{1}{2}\left(\begin{bmatrix} \mathbb{I} \\ -{\frac{\partial \phi}{\partial f}}^{+}\frac{\partial \phi}{\partial q_a} \end{bmatrix}\dot{q}_a\right)^T M\left(\begin{bmatrix} \mathbb{I} \\ -{\frac{\partial \phi}{\partial f}}^{+}\frac{\partial \phi}{\partial q_a} \end{bmatrix}\dot{q}_a\right) \tag{7}$$

Then by analogy:

$$M_a = \begin{bmatrix} \mathbb{I} \\ -{\frac{\partial \phi}{\partial f}}^{+}\frac{\partial \phi}{\partial q_a} \end{bmatrix}^T M \begin{bmatrix} \mathbb{I} \\ -{\frac{\partial \phi}{\partial f}}^{+}\frac{\partial \phi}{\partial q_a} \end{bmatrix} \tag{8}$$

This leads to the generalization of the effective inertia in the presence of closed-loop constraints:

$$\Lambda_A = (J_A M_a^{-1} J_A^T)^{-1} \tag{9}$$

III. Evaluation criteria

We propose several performance criteria of leg design accounting for parallel architectures. The proposition is based on our understanding of which properties are expected from a walking machine: Its foot must move fast, with low apparent inertia and good shock absorption capability. It should easily compensate for its own weight and should be compact.

A. Velocity manipulability

The manipulability of a robot [24] can be seen as the ellipsoid of speed the effector can produce with constant unit joint velocity $\dot{q}^T\dot{q} = 1$. For parallel architectures, only the motor coordinates can be controlled, so we need to rewrite it as $\dot{q}_a^T\dot{q}_a = 1$, which leads to the equivalent ellipsoid given by $v^T(J_A J_A^T)^{-1}v = 1$. While J_A carries information about translational and rotational movements, we prefer to separate the manipulability between translation and rotation, with $J_A = [Jt_A^T, Jr_A^T]^T$. This gives two manipulability criteria:

$$TM = det(Jt_A Jt_A^T) \tag{10}$$

$$RM = det(Jr_A Jr_A^T) \tag{11}$$

With TM and RM, the translation and rotation manipulability indexes, reflecting the volume of the ellipsoids of translational and rotational velocities. These criteria give the global kinematic capability and do not reflect in which direction the robot foot can achieve the highest velocity. As the leg will mainly need to transmit force on the z-axis, this particular direction is studied with its own criteria.

B. The z-reduction ratio

We next characterize the capability of the system to transmit low vertical effort to the actuators. In quasi-static, the actuator forces τ_a can be expressed as a function of the ground reaction force on the foot $\lambda_A \in se(3)^*$:

$$\tau_a = J_A^T\lambda_A \tag{12}$$

We define the z-reduction ratio (ZRR) as the norm of the projection of J_A on the z-axis.

$$ZRR = \|Jt_A^T z\| \tag{13}$$

The norm is investigated here to penalize multiple motors that must produce torque to compensate for a z-axis force and to maintain the robot up. Low ZRR is desirable and is somehow antagonist to high translation manipulability in z.

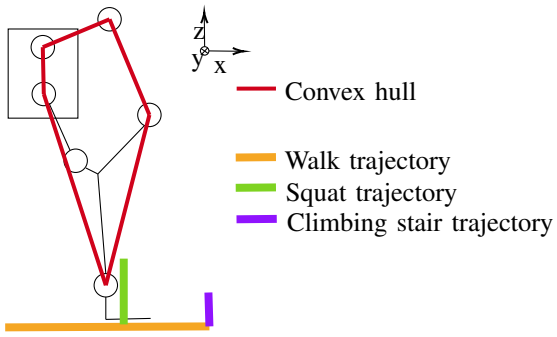

Fig. 2. Convex hull and trajectory example

C. Compactness

The compactness of the design must be quantified, as an important footprint may hinder the capability of the biped to navigate in cluttered environments. An easy way to evaluate the volume V_3 occupied by the leg is to compute the convex hull of the leg, as depicted in Fig. 2. In this study, we only consider the hull at the center of the joints. As the leg will mainly move on the sagittal plane ((xz) in Fig. 2), we additionally consider V_2 the area of the convex hull projected on this plane.

D. Foot Effective Inertia

An agile biped robot should have light legs, especially on the vertical axis to generate dynamic motion. We therefore mainly characterize the foot effective inertia along the z-axis. The z-axis inertia (ZAI) index is:

$$ZAI = [z,0]\Lambda_A[z,0]^T \tag{14}$$

It should be as low as possible to get an optimal robot. Since the leg is globally oriented on z, we argue that minimizing the ZAI will impact more joints and links of the leg than globally evaluating the foot inertia.

E. Impact mitigation factor

The impact mitigation factor (IMF) was introduced [16] to characterize the shock absorption capability. It compares how the entire floating system reacts to external forces, to its reaction when the basis is fixed. Due to space limits, we briefly report here how to extend it to parallel kinematics. The apparent inertia Λ_A was computed for the fixed-basis mechanism. The exact same developments for the floating-basis mechanism lead to the free-basis apparent foot inertia, noted $\Lambda_{A_{free}}$, and the free basis apparent foot inertia when the leg is locked, noted $\Lambda_{A_{lock}}$. Following [16], the IMF then is:

$$IMF = det(\mathbb{I} - \Lambda_{A_{free}}\Lambda_{A_{lock}}^{-1}) \tag{15}$$

IV. Studied bipedal robots

We evaluate the relevance of our metrics on five representative designs of bipedal legs, chosen from the literature and displayed in Fig. I. As several are not reported with accessible open-source description format, we have built the five corresponding open-source packages scaled into similar dimensions. These descriptions have been gathered using the main available data, as explained below, with inertia deduced from uniform equivalent materials. The CAD models are available on GitHub[1]. Even though some of the studied designs are not inspired by biology, a unified vocabulary is used to describe them. The hip will designate the 3 degrees of freedom, which generate the rotation close to the torso; the knee will designate, if possible, the next degree of freedom placed after the hip, then the ankle will designate the 2 rotational degrees of freedom of the foot.

Furthermore, the transmission systems of the robots and their additional inertia are not modeled here, as we are not evaluating these components in the proposed criteria and let it for further work.
[1]

1) Digit: Digit[4] is a serial-parallel bipedal robot with 6 dof on each leg. **Kinematics:** It adopts a serial-parallel architecture where the 3 dof of the hip are placed in serial. The knee actuation is deported close to the hip, thanks to a rod. The last two dof of the ankle are driven by two motors deported near the knee thanks to two rods. **Actuation:** Each one of the 6 motorized joints of this leg is in quasi-direct drive. **Loop closure:** It compounds 3 closed loops per leg. One for the actuation of the knee and two for the actuation of the ankle. In the CAD, each rod is cut in half, and a 6d constraint is set between each two parts.

2) Talos: Talos [19] is a serial robot with 6 dof on each leg. **Kinematics:** It adopts a serial architecture, with the dorsiflexion of the ankle deported inside the shin thanks to a parallelogram linkage. **Actuation:** Each one of the 6 motorized joints are actuated by a motor with a harmonic gearing. **Loop closure:** It has one closed loop on each leg inside the parallelogram. In the CAD, one rod is cut in half, and a 6d constraint is set between its two parts.

3) Kangaroo: Kangaroo [5] is a serial-parallel bipedal robot with 6 dof on each leg. **Kinematics:** It adopts a serial-parallel architecture where the supination of the hip is actuated by one linear motor, and the abduction and the flexion are set in parallel thanks to two rods controlling a universal joint. The knee is controlled by one actuator, and the two dof of the ankle are controlled by two actuators placed near the hip, which transmit their movement through two rods and a referral triangle controlling the universal joint of the ankle. **Actuation:** Each one of the 6 motorized joints is a prismatic joint made from a ball-screw transmission system to generate translational movement. **Loop-closure:** It compounds 11 closed loops by leg. Most of them are due to the usage of translational motors. In the CAD, each rod is cut in half, and the 6d constraint is set between each two parts.

4) Disney Bipedal Robot: The Disney Bipedal[21] Robot is a serial-parallel bipedal robot with 6 dof on each leg. **Kinematics:** It adopts a serial-parallel architecture where the

[1] https://gitlab.laas.fr/vbatto/closed_loop_kinematics_pinocchio

abduction of the hip is actuated by one motor. The supination, flexion of the hip, knee flexion, and ankle inversion are set in parallel thanks to two 5-bar linkages. The dorsiflexion of the ankle is directly controlled by a motor placed on the foot. **Actuation:** Each one of the 6 motorized joints is driven by a servo motor. **Loop-closure:** It compounds 3 closed loops: one on each 5-bar linkage and one between the two 5-bar linkages. In the CAD, 3 rods are cut in half, and a 6d constraint is placed between each two parts.

5) WL16: WL16 [20] is a parallel bipedal robot with 6 dof on each leg. **Kinematics:** Each leg has the fully parallel structure of a Gough-Stewart platform [26]. **Actuation:** Each one of the 6 motorized joints is a prismatic joint made from an electric cylinder. **Loop-closure:** It compounds 5 closed loops, on 5 of the 6 cylinders. In the CAD, the pistons of these 5 cylinders are cut in half, and a 6d constraint is made between each part.

V. Quantitative evaluation and discussion

We do not aim here at comparing each leg to the others. Indeed, each architecture is fundamentally different and might have been designed with respect to different goals. We rather seek to validate the criteria and corroborate them with what we know of the characteristics and achievements of the 5 considered robots.

A. Reference trajectories

The benchmark is based on 3 simple reference trajectories defined in operational space and presented in Fig 2[2].

- A 40cm forward movement of the foot wrt the hip, corresponding to a walking step.
- A 20cm upward movement of the foot wrt the hip, corresponding to a squat.
- A corner movement (16cm forward then 20cm upward wrt the hip), corresponding to the climb of a stair.

These 3 trajectories correspond to common use cases of a bipedal robot. The lengths are set to cover the range of motion that an average robot can do, with a standardized leg height of 80cm. From these 3 references, a collection of trajectories is obtained by randomizing the displacement, chosen so that the standard deviation around the nominal reference is 2.5cm

B. Motion generation

The motion of the robot model is finally obtained by implementing a simple cartesian regulator around the reference trajectories.

Each trajectory is discretized in a set of 100 positions, and to rapidly model the robots, each desired trajectory is tracked by the foot, thanks to the closed-loop Jacobian. The velocity of the actuated joints is set to:

$$\dot{q}_a = J_A^{\dagger} v_A^* \tag{16}$$

With $v_A^* \in se(3)$, the reference velocity of our operational frame $\mathscr{F}_A$ (foot tip) set to correct the error wrt the reference trajectory. The velocity of the entire leg (free and actuated joints) is then:

$$\dot{q} = \frac{\partial q}{\partial q_a} \dot{q}_a \tag{17}$$

This velocity is then integrated to obtain the joint trajectory and clipped to stay within the joint limits. We arbitrarily define the joint limits to avoid non-mountable configurations, as discussed in Sec. II-A. For the WL16, we set the bounds of the cylinders to a maximal extension of 150% of their minimal length.

The resulting trajectories are discretized into 100 configurations each. Each criterion is computed on each of these samples. The computation is made with Python and the Pinocchio library [27].

C. Scaling

We have separated translation TM and rotation RM manipulability to avoid the scaling effect due to mixing lengths and angles. Yet most of the criteria are based on Jacobians, and are subject to the same issue due both to prismatic and revolute joints, and to translation and rotation of the effector. In practice, we suggest to introduce a scaling factor to obtain adimensional (unit-free) Jacobians. Alternatively, attention may be paid to the unit used for each dimension, but it would negatively affect the genericity of the approach.

The approach applies to any Jacobian J split into a translational and a rotational component, $J^T = [J_t^T, J_r^T]$. We denote the i^{th} column with $[i,:]$ Depending on the type of the joint corresponding to Column i, we have:

$$\langle Jt[i,:] \rangle = \begin{cases} \langle . \rangle & \text{if Joint } i \text{ is prismatic} \\ \langle m \rangle & \text{else} \end{cases} \tag{18}$$

$$\langle Jr[i,:] \rangle = \begin{cases} \langle m^{-1} \rangle & \text{if Joint } i \text{ is prismatic} \\ \langle . \rangle & \text{else} \end{cases} \tag{19}$$

where $\langle - \rangle$ stands for the unit of the corresponding quantity (meter, adimensional or meter-inverse here).

To obtain an adimensional Jacobian, we choose to scale it by multiplying the translation part and rotation part of the Jacobian by two diagonal matrices D_t, D_r, following [23]. We choose the scaling matrices D so that they make the unit of the Jacobians invariant to joint type, i.e.:

$$D_t = diag(d_i) \text{ with } d_i = \begin{cases} 1 & \text{if Joint } i \text{ is prismatic} \\ d_t & \text{else} \end{cases}$$

$$D_r = diag(d_i) \text{ with } d_i = \begin{cases} d_r & \text{if Joint } i \text{ is prismatic} \\ 1 & \text{else} \end{cases}$$

To cancel the scaling effect, the weight d_t is chosen as the mean of the singular values of the matrix J_t where only the columns corresponding to the revolute joints are selected (i.e. only the terms of unit $\langle m \rangle$ in (18)). Respectively, d_r is the mean of the singular values of the prismatic columns of J_r (i.e. the terms of unit $\langle m^{-1} \rangle$ in (19)). The scaling factors D_t and D_r then account for all the lengths present inside the architecture. The scaled adimensional Jacobian $\bar{J}$, invariant to joint-type dimension is finally:

$$\bar{J} = \begin{bmatrix} JtD_t \\ JrD_r \end{bmatrix} \tag{20}$$

[2]See the companion video, available at `https://peertube.laas.fr/w/9HoFdHzhHQNfMJrbJxu2F1`

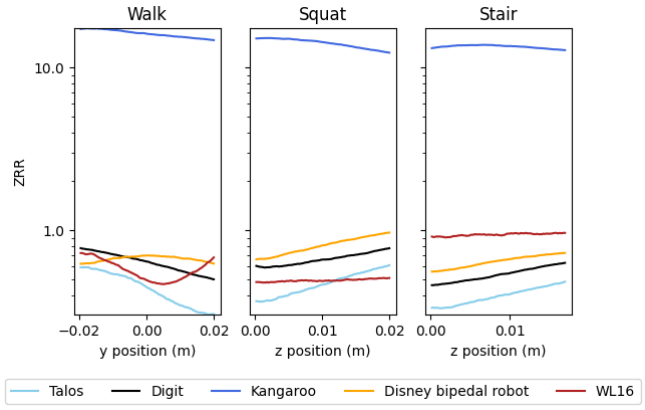

Fig. 3. Z-reduction ration (ZRR)

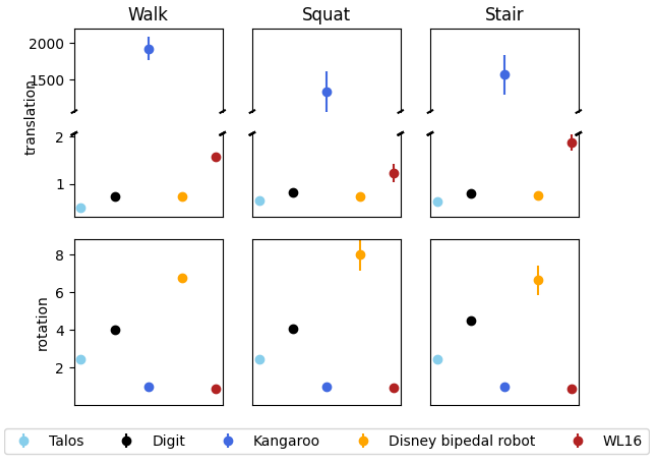

Fig. 4. Velocity manipulability of the foot, in translation (TM, top) and rotation (RM, bottom)

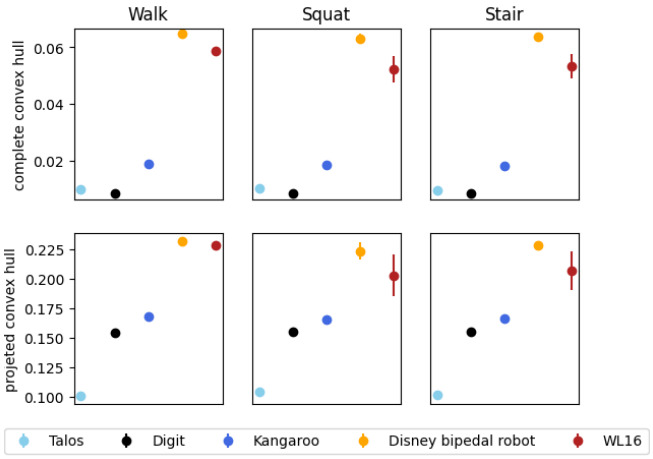

Fig. 5. Leg convex hull in volum V_3 (top) and sagittal area V_2 (bottom)

The adimensional manipulability $\overline{\text{TM}}$, $\overline{\text{RM}}$, and the ration $\overline{\text{ZRR}}$ are then computed from the scaled Jacobian:

$$\begin{aligned} \overline{\text{TM}} &= det(Jt_A {D_t}^2 Jt_A^T) \\ \overline{\text{RM}} &= det(Jr_A {D_r}^2 Jr_A^T) \\ \overline{\text{ZRR}} &= ||D_t Jt_A^T \vec{z}|| \end{aligned} \tag{21}$$

As only the adimensional version of these criteria will be used in what follow, TM, RM and ZRR now abusively refer to these values.

D. Analysis and discussion

1) Z-reduction ratio : The ZRR for each robot and each movement are plotted in Fig. V-D.1. Over the different trajectories, the ZRR stays relatively constant and small, except for the robots that use prismatic actuation. The variation is noticeable for WL16, but particularly remarkable for Kangaroo. Its ZRR is 10 times larger than other robots.The large ZRR of Kangaroo is compensated by the use of a ball-screw transmission system to generate translational movement. This result highlights the relevance of the ZRR, as all these robots are largely capable of withstanding vertical reaction forces.

2) Velocity manipulability: The TM and RM values are shown in Fig. 4. The translation manipulability of Kangaroo is significantly higher than for any other robot. This reflects the particular architecture of this robot, which only requires small actuator displacements to produce all the robot reference trajectories. The rotation manipulability of all the studied robots is similar. Only the Disney robot shows a slight improvement in rotational velocity capabilities. As rapid foot rotations are not expected on a biped, it is likely that it is a side effect of the ankle actuation rather than a careful decision optimized during the design process.

3) Compactness: The compactness criteria are displayed in Fig. 5. On the top row, the occupancy volume V_3 of all 5 robots is similar and very low, though the WL16 and Disney bipedal robots tend to span more space over the reference movements. This reflects their general architecture choices, which rely on parallelism more systematically than the others, in particular with no main hip-knee-ankle serial chain. Since the WL16 is not a planar architecture, it takes more space. The Disney bipedal robot loses compactness because of its two five-bar linkages.

The anteroposterior projected convex hull V_2 (sagittal area) is presented in Fig. 5 (bottom). It highlights that parallel architectures such as Digit or Kangaroo tend to occupy more space than serial ones such as Talos. This result validates the relevance of this criterion, in particular when optimizing the volume spanned by an architecture.

4) Relevance of the proposed inertia model: We first recall that each robot part/link is modeled as to be made of plain plastic with a density of $1g/cm^3$ for each structural part, and plain material with a density of $4g/cm^3$ (half the steel) for the motor part. These assumptions correspond to the mean density of structural and motor parts. We first validate with Table I the relevance of this hypothesis, by comparing our average-inertia model with the open-source ground-truth model of Talos [19].

The error induced by our simplest modeling hypothesis is rather limited, and is not likely to significantly change the predicted behavior and the relevance of this study.

	tighs mass	shin mass	foot mass
Open source Talos	6.8kg	3.6kg	1.6kg
modelized Talos	5.8kg	3.12kg	2.4kg

TABLE I

MASS OF TALOS PIECES ON DIFFERENT MODEL

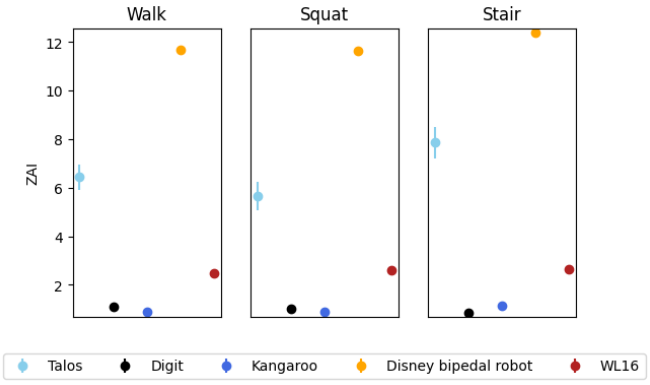

Fig. 6. z-apparent inertia (ZAI) of the foot

5) Apparent inertia: The ZAI of the foot of each robot is presented in Fig. 6. As expected, Talos and the Disney bipedal robot have important leg-effective inertia due to the presence of a motor on the foot. Every other robots with small motors (Digit) or no motors (Kangaroo and WL16) embedded in the leg have a small inertia. The important inertia of the Disney bipedal robot is strongly due to the scaling of the robot, while the robot was optimized with a leg size of only about 40cm. Nevertheless, this criterion highlights the need to reduce the mass near the foot.

6) Impact Mitigation Factor: To compute the impact mitigation factor, the mass of each torso is set at 40kg. The global IMF is presented in Fig. 7. The isotropic IMF is displayed on the top row and is nearly null for all robots except WL16. Indeed, none of the reported architecture is explicitly designed to absorb impacts. WL16 higher IMF is a side-effect of its architecture, as it is derived from a Stewart platform, providing a more isotropic behavior.

These legged machines are rather expected to absorb shock in the z direction when the robot walks/runs/jumps. When we look at the IMF projected on the z-axis (Fig. 7, bottom), the results are much better for every robot. On the z-axis, the WL16 presents high impact-absorption performance, closely followed by Digit, which also shows to absorb impact efficiently. The Disney bipedal robot and Talos have a lower impact-mitigation capability, undoubtedly due to the presence of the big ankle actuators directly on the foot.

We point out here that the inertia of the actuators is not modeled in the proposed library (only the added masses of the motors are modeled, not the apparent inertia induced, e.g., by the rotor inertia multiplied by the reduction ratio). This would likely change the values, in particular for Talos. Yet the results confirm the relevance of the IMF in evaluating the dynamic capabilities of an architecture.

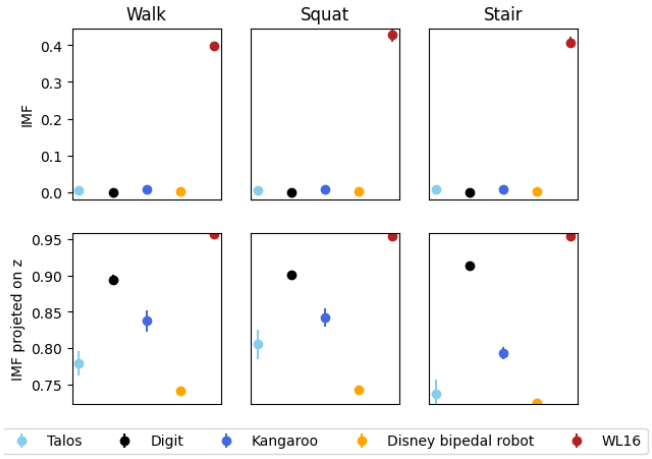

Fig. 7. Impact mitigation factor (IMF), isotropic (top) and in z (bottom)

VI. CONCLUSION

This paper proposed a set of new criteria to systematically characterize the design of a bipedal robot leg. These criteria include manipulability, the Z Reduction Ratio, the Z-Axis Inertia, the Impact Mitigation Factor, and the leg convex hull. These criteria can be used to design an efficient leg with a minimal ZRR, a maximal TM, and RM. A Dynamic leg with a minimal ZAI and a maximal IMF or Compact leg with a minimal convex hull.

We also provided the formulations to compute these criteria with any serial or parallel architecture, accounting for the most generic model with implicit constraints.

We have shown the relevance of these criteria by applying them to discuss the performance of 5 existing robots representing the main classical architectures of the literature. This implied to reproduce the 5 CAD models in a consistent scaling and format that we also propose in open source.

This study has successfully demonstrated the effectiveness of the proposed criteria in evaluating the leg design. We argue that they cover the main aspects of the kinematic design, accounting for the ability to quickly move (TM, RM), sustain ground reaction forces (ZRR), react (ZAI), absorb shocks (z-IMF), and navigate in cluttered environments (convex hull V_2). The results obtained from the application of these criteria to the selected robots have provided valuable insights into their architectural designs and the overall performance of bipedal robots.

We have limited our study to the kinematic model without yet modeling the actuation and characterizing it. This would need additional criteria, likely considering the full dynamic model and not only the inertia. However, this limitation does not invalidate the proposed criteria but simply calls for an additional batch of them. Finally, the overall objective of our contribution is to set the basis for a systematic optimization of the kinematics of biped legs, which we consider doing next.

REFERENCES

[1] [1J. Pratt et B. Krupp, Design of a bipedal walking robot , présenté à SPIE Defense and Security Symposium, Orlando, FL, G. R. Gerhart, D. W. Gage, et C. M. Shoemaker, Éd., Orlando, FL, avr. 2008, p. 69621F. doi: 10.1117/12.777973.

[2] J. W. Grizzle, J. Hurst, B. Morris, H.-W. Park, et K. Sreenath, MABEL, a new robotic bipedal walker and runner , in 2009 American Control Conference, St. Louis, MO, USA: IEEE, 2009, p. 2030-2036. doi: 10.1109/ACC.2009.5160550.

[3] G. Figliolini, M. Ceccarelli, et M. Di Gioia, Descending stairs with EP-WAR3 biped robot , in Proceedings 2003 IEEE/ASME International Conference on Advanced Intelligent Mechatronics (AIM 2003), Kobe, Japan: IEEE, 2003, p. 747-752. doi: 10.1109/AIM.2003.1225436.

[4] Agility Robotics. (2019) Digit advanced mobility for the human world. [Online]. Available: https://www.agilityrobotics.com/robotsdigit

[5] ROIG, Adria, KOTHAKOTA, Sai Kishor, MIGUEL, Narcis, et al. On the hardware design and control architecture of the humanoid robot kangaroo. In: 6th Workshop on Legged Robots during the International Conference on Robotics and Automation (ICRA 2022). 2022.

[6] E. Guizzo, "By leaps and bounds: An exclusive look at how Boston dynamics is redefining robot agility," in IEEE Spectrum, vol. 56, no. 12, pp. 34-39, Dec. 2019, doi: 10.1109/MSPEC.2019.8913831.

[7] J. Reher, W.-L. Ma, et A. D. Ames, Dynamic Walking with Compliance on a Cassie Bipedal Robot, in 2019 18th European Control Conference (ECC), Naples, Italy: IEEE, juin 2019, p. 2589-2595.

[8] J. A. Grimes et J. W. Hurst, THE DESIGN OF ATRIAS 1.0 A UNIQUE MONOPOD, HOPPING ROBOT, in Adaptive Mobile Robotics, WORLD SCIENTIFIC, 2012, p. 548-554.

[9] S. Amstutz et A. A. Novotny, Topological optimization of structures subject to Von Mises stress constraints, Struct Multidisc Optim, vol. 41, n 3, p. 407-420, avr. 2010, doi: 10.1007/s00158-009-0425-x.

[10] T. Dinev, C. Mastalli, V. Ivan, S. Tonneau, et S. Vijayakumar, A Versatile Co-Design Approach For Dynamic Legged Robots , in 2022 IEEE/RSJ International Conference on Intelligent Robots and Systems (IROS), Kyoto, Japan: IEEE, oct. 2022, p. 10343-10349. doi: 10.1109/IROS47612.2022.9981378.

[11] L. Stocco, S. E. Salcudean, et F. Sassani, Fast constrained global minimax optimization of robot parameters, Robotica, vol. 16, n 6, p. 595-605, nov. 1998, doi: 10.1017/S0263574798000435.

[12] J. Angeles et F. C. Park, Performance 10. Performance Evaluation and Design Criteria, Springer Handbook of Robotics, 2008.

[13] R. Unal, G. Kiziltas, et V. Patoglu, Multi-criteria Design Optimization of Parallel Robots, in 2008 IEEE Conference on Robotics, Automation and Mechatronics, Chengdu: IEEE, sept. 2008, p. 112-118. doi: 10.1109/RAMECH.2008.4681427.

[14] R. S. Stoughton et T. Arai, A modified Stewart platform manipulator with improved dexterity, IEEE Trans. Robot. Automat., vol. 9, n 2, p. 166-173, avr. 1993, doi: 10.1109/70.238280.

[15] G. Fadini, T. Flayols, A. Del Prete, N. Mansard, et P. Soueres, Computational design of energy-efficient legged robots: Optimizing for size and actuators, in 2021 IEEE International Conference on Robotics and Automation (ICRA), Xi'an, China: IEEE, mai 2021, p. 9898-9904. doi: 10.1109/ICRA48506.2021.9560988.

[16] WENSING, Patrick M., WANG, Albert, SEOK, Sangok, et al. Proprioceptive actuator design in the mit cheetah: Impact mitigation and high-bandwidth physical interaction for dynamic legged robots. Ieee transactions on robotics, 2017, vol. 33, no 3, p. 509-522.

[17] D. E. Orin et A. Goswami, Centroidal Momentum Matrix of a humanoid robot: Structure and properties , in 2008 IEEE/RSJ International Conference on Intelligent Robots and Systems, Nice: IEEE, sept. 2008, p. 653-659. doi: 10.1109/IROS.2008.4650772.

[18] MERLET, Jean-Pierre. Parallel robots. Springer Science & Business Media, 2006.

[19] STASSE, Olivier, FLAYOLS, Thomas, BUDHIRAJA, Rohan, et al. TALOS: A new humanoid research platform targeted for industrial applications. In: 2017 IEEE-RAS 17th International Conference on Humanoid Robotics (Humanoids). IEEE, 2017. p. 689-695.

[20] LIM, Hun-ok et TAKANISHI, Atsuo. Biped walking robots created at Waseda University: WL and WABIAN family. Philosophical Transactions of the Royal Society A: Mathematical, Physical and Engineering Sciences, 2007, vol. 365, no 1850, p. 49-64.

[21] GIM, Kevin G., KIM, Joohyung, et YAMANE, Katsu. Design and fabrication of a bipedal robot using serial-parallel hybrid leg mechanism. In: 2018 IEEE/RSJ International Conference on Intelligent Robots and Systems (IROS). IEEE, 2018. p. 5095-5100.

[22] Roy Featherstone. 2007. Rigid Body Dynamics Algorithms. Springer-Verlag, Berlin, Heidelberg.

[23] Khan, S., Andersson, K. Wikander, J. Jacobian Matrix Normalization - A Comparison of Different Approaches in the Context of Multi-Objective Optimization of 6-DOF Haptic Devices. J Intell Robot Syst 79, 87–100 (2015).

[24] YOSHIKAWA, Tsuneo. Manipulability of robotic mechanisms. The international journal of Robotics Research, 1985, vol. 4, no 2, p. 3-9.

[25] KHATIB, Oussama. Commande dynamique dans l'espace opérationnel des robots manipulateurs en présence d'obstacles. PhD dissertation, Ecole Nationale Superieure de l'Aeronautique et de l'Espace, 1980.

[26] DASGUPTA, Bhaskar et MRUTHYUNJAYA, TS1739334. The Stewart platform manipulator: a review. Mechanism and machine theory, 2000, vol. 35, no 1, p. 15-40.

[27] CARPENTIER, Justin, SAUREL, Guilhem, BUONDONNO, Gabriele, et al. The Pinocchio C++ library: A fast and flexible implementation of rigid body dynamics algorithms and their analytical derivatives. In: 2019 IEEE/SICE International Symposium on System Integration (SII). IEEE, 2019. p. 614-619.

[28] CARPENTIER, Justin, BUDHIRAJA, Rohan, et MANSARD, Nicolas. Proximal and sparse resolution of constrained dynamic equations. In: Robotics: Science and Systems 2021. 2021.

[29] BEN-ISRAEL, Adi et GREVILLE, Thomas N. Generalized inverses: theory and applications. Springer, 2003.